Using a Map of Measurement Noise to Improve UWB Indoor Position Tracking

William Suski, *Student Member, IEEE,* Salil Banerjee, *Student Member, IEEE,* and Adam Hoover, *Senior Member, IEEE*

***Abstract*—Ultrawideband signals present new opportunities for indoor position tracking due to their ability to operate in non-line-of-sight conditions. However, walls and other normal indoor infrastructure cause a systemic spatial warp in the measurements. In this paper, we describe methods to manually build a map of the measurement noise and use it in a particle filter framework to improve measurement accuracy. We tested our methods in two facilities, collecting over 5.6 million measurements. Evidence shows that the measurement noise is multimodal, location dependent, stable over time, and locally similar. Using the map in a particle filter framework, we demonstrate an average improvement in measurement accuracy of 30%.**

***Index Terms*—Indoor ranging, noise model, particle filter, position estimation, ultrawideband (UWB).**

I. Introduction

An ULTRAWIDEBAND (UWB) positioning system works by estimating the range and/or angle from multiple fixed points to a mobile terminal [1]. This set of measurements is then used to calculate position through multilateration or multiangulation [2]. The position measurements are subject to noise caused by several sources including the system installation geometry, discrepancies in system synchronization, non-line-of-sight (NLOS) conditions, and multipath [3]. While many of these noise sources have been studied independently [4]-[5], the quality of the noise of the final position estimates has received little attention. In this context, it is important to note the difference between improving individual range measurements and improving the overall position measurement. A position measurement is the output of multilateration or multiangulation that uses a combination of multiple range measurements. In this paper, we describe methods to systematically build a spatial map of position measurement noise throughout the area in which the UWB system is operating. We then demonstrate the use of this map in a particle filter to improve position measurement accuracy.

Several noise sources for UWB measurements have been previously investigated. Accuracy has been shown to improve by averaging multiple measurements [4], by signal pulsing [6], and through methods that improve peak detection of individual range estimates [7], [8]. Multipath interference and tag synchronization were investigated in [9], and accuracy was improved through direct down conversion and an iterative peak subtraction algorithm. Zhou *et al.* [10] developed a system that avoids synchronization issues using a fixed, known locator transmitter along with the target transmitter. NLOS detection and mitigation techniques have also been developed [11]–[13]. Minimizing the error caused by sensor geometry has been previously considered in [14] and [15]. While all of these methods can improve UWB measurement accuracy, it is reasonable to assume that some amount of error will still occur, especially in challenging indoor environments where multipath and NLOS are the rule rather than the exception [5]. Fig. 1 illustrates the effect of a systemic warp in the measurement noise caused by this type of environment.

Maps are a well-known resource for improving measurement accuracy for a variety of instruments. In indoor tracking, maps have been used for creating location fingerprints. The idea is to create a database of measurement properties for locations as part of the calibration process. Live measurements are then compared against the database and location is estimated using pattern matching techniques. For example, a map of magnetic field strength measurements is used in [16] to perform indoor localization. Steiner and Wittneben [17] present a method that uses a collection of UWB energy measurements as a location fingerprint. A similar method is described in [18] for localization within an area covered by a wireless local area network. Maps have also been used as landmark references for improving tracking. For example, road maps have been shown to improve tracking accuracy for automobiles [19] and are now commonly used in commercial GPS systems. A database of terrain distance measures has been shown to improve surface and underwater ship navigation accuracy [20]. Building floor plans have been used to constrain tracks from passing through walls [21], [22].

In this paper, we propose to systematically build a map of position measurement noise for an indoor UWB system, and then use that map to improve measurement accuracy. We describe methods to measure the noise in a grid-like fashion and mathematically model it. We then develop a particle filter that uses the map to mitigate the effect of the measurement noise. Although we demonstrate our methods only on an

Manuscript received July 17, 2012; revised October 24, 2012; accepted November 26, 2012. Date of publication May 6, 2013; date of current version July 10, 2013. This work was supported in part by the Office of Naval Research (ONR) under Grant N00014-07-1-1001. The Associate Editor coordinating the review process was Dr. Jesús Ureña.

The authors are with the Department of Electrical and Computer Engineering, Clemson University, Clemson, SC 29634 USA (e-mail: wsuski@clemson.edu; salilb@clemson.edu; ahoover@clemson.edu).

Digital Object Identifier 10.1109/TIM.2013.2256714

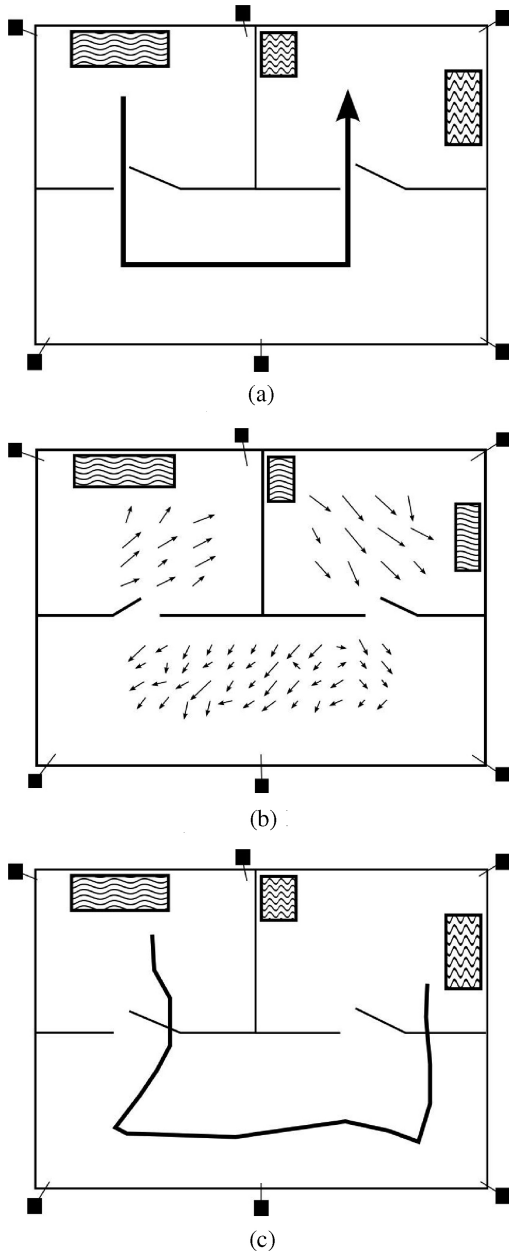

Fig. 1. Illustration of systemic noise on UWB position measurements in an indoor facility. Sensors are indicated by the black squares and furniture by the shaded rectangles. (a) Actual motion. (b) Measurement noise. (c) Raw measurements.

indoor UWB positioning system, we believe they could be applied to other instruments that exhibit similar systemic warped measurement noise.

II. Methods

A. Test Facilities

Measurements were collected in two different test facilities. The first is approximately 13 × 10 m, and was built as part of the Military Operations in Urban Terrain (MOUT) project at Clemson University [23], [24]. It consists of a painted concrete slab floor, a number of polyvinyl chloride (PVC) walls, and an exposed steel roof. Ten UWB receivers are distributed throughout the test area. A 2-D floor plan of the area is shown in Fig. 2.

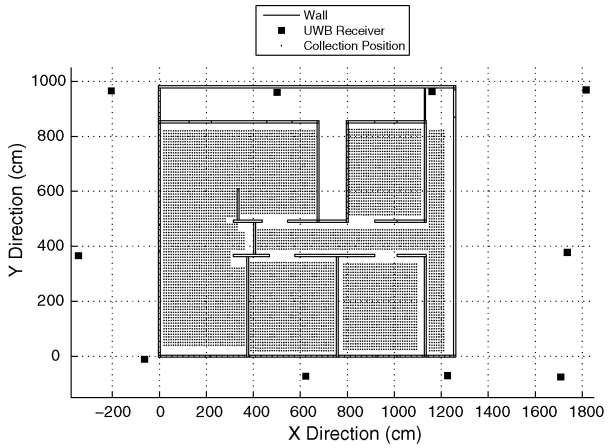

Fig. 2. Floor plan of the Shoothouse facility. Filled squares indicate sensor locations. Unfilled squares indicate locations surveyed. Solid lines indicate walls.

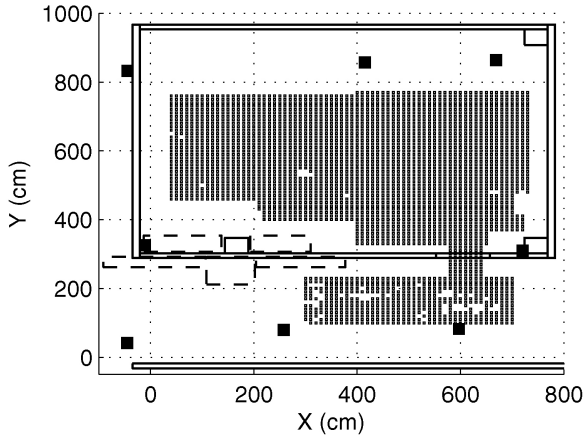

Fig. 3. Floor plan of the Riggs facility.

The second test facility encompasses part of a hallway and an open lab space. The installation was designed so that the measurement noise would be similar to that of a standard office environment. It is an approximately 8 × 8 m area of Clemson University's Riggs Hall and consists of a concrete floor covered with vinyl tile or carpet. Eight UWB receivers are distributed throughout the test area. A block wall runs through the test area, dividing the main room (upper section) from the corridor (lower section). A 2-D floor plan of the area is shown in Fig. 3.

B. UWB System

Our UWB system was developed by Ubisense (http://www.ubisense.net). Mobile Ubisense tags transmit UWB pulses that are detected by the fixed sensors. Range estimates to the tags are determined using angle of arrival and time-difference of arrival techniques that allow the system to calculate position estimates with as few as two sensors reporting measurements [25], [26]. The system is capable of tracking multiple tags simultaneously using a time-division multiple access technique similar to that described in [27].

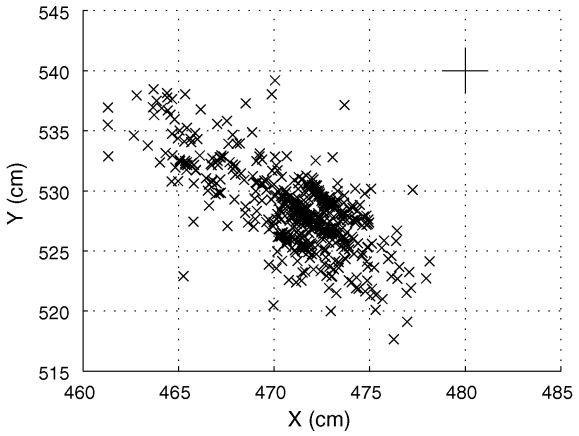

Fig. 4. Measurements taken at location (480, 540) cm.

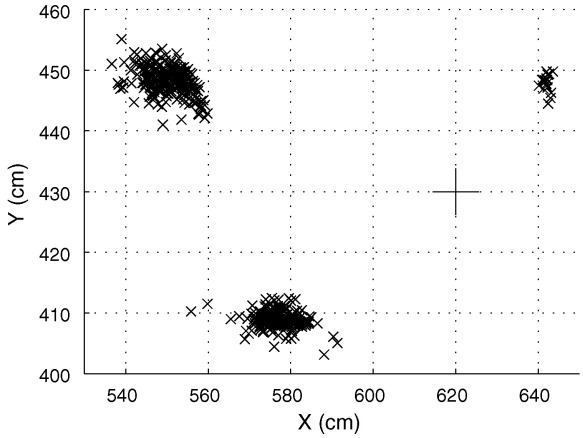

Fig. 5. Measurements taken at location (620, 430) cm.

The sensors are fixed at known locations in a relative coordinate system defined within the test facilities. The origin of each is located in the bottom left corners of Figs. 2 and 3. The relative location of each sensor was determined using tape measures, laser squares, and laser distance measurement tools. These ground truth sensor locations are used by the Ubisense system to calculate tag location.

C. Measurement Collection

To gain knowledge of the overall measurement noise affecting this type of installation, position measurements were taken in a dense grid throughout each test facility. The ground truth positions were determined relative to the coordinate system and in the same manner as discussed for the sensors in Section II-B. Based on the methods used to determine these ground truth locations, the coordinate system is believed to be accurate to within 1 cm. Figs. 2 and 3 denote the collection locations with unfilled squares. Measurements were taken at 7931 locations in the Shoothouse facility and 3272 locations in the Riggs facility. A space of 10 cm separates each collection location and 500 measurements were collected at each location. A total of approximately 5.6 million measurements were taken. A number of gaps can be seen in the collection locations shown in Fig. 3. These are the locations where the tracking system did not regularly report positions due to the installation.

Fig. 4 shows an example set of 500 measurements collected at (480, 540) cm within the Riggs facility. This data forms a distinct cluster and is largely shifted down and to the left from the ground truth location denoted by the large cross symbol. Fig. 5 shows another set of 500 measurements collected at (620, 430) cm within the Riggs facility. This data is different from that of Fig. 4 because it clearly forms multiple clusters. Across both facilities, the majority of locations showed measurement noise similar in quality to that shown in Figs. 4 and 5, with a number of distinct clusters varying from one to as many as eight.

D. Measurement Noise Model

We assume that each position measurement is corrupted by measurement noise sampled from a 2×1 random vector $\boldsymbol{\nu}$, given by

$$\boldsymbol{\nu} = \begin{bmatrix} \nu_x \\ \nu_y. \end{bmatrix} \tag{1}$$

This assumption leads to the set of measurement equations $\mathbf{g}$ shown in (2) where x_t and y_t are the actual location and $z_{x,t}$ and $z_{y,t}$ are the estimates provided by the UWB system at time t

$$\mathbf{z}_t = \mathbf{g}(\mathbf{x}_t, \boldsymbol{\nu}_t) = \begin{bmatrix} z_{x,t} = x_t + \nu_{x,t} \\ z_{y,t} = y_t + \nu_{y,t}. \end{bmatrix}. \tag{2}$$

Based on our 5.6 million observations, we adopted a weighted mixture of Gaussians as the model for measurement noise [28]. The measurement noise $\boldsymbol{\nu}$ is assumed to be a bivariate, mixture of Gaussian random variables (RV). The probability density function (PDF) of this type of RV is made up of weighted PDFs of multiple unimodal, bivariate Gaussian RVs and described by (3). This PDF is often referred to as a mixture of Gaussians [29]. This equation has five parameters for each mode: the means, $\mu_{x,i}$ and $\mu_{y,i}$, the standard deviations, $\sigma_{x,i}$ and $\sigma_{y,i}$, and the correlation coefficient, $\rho_{x,y,i}$

$$p_i(z_x, z_y|x, y) = \frac{1}{2\pi\sigma_{x,i}\sigma_{y,i}\sqrt{1-\rho^2_{x,y,i}}} \exp \left(\frac{-1}{2(1-\rho^2_{x,y,i})} \left[\frac{(z_x-\mu_{x,i})^2}{\sigma^2_{x,i}} + \frac{(z_y-\mu_{y,i})^2}{\sigma^2_{y,i}} - \frac{2\rho_{x,y,i}(z_x-\mu_{x,i})(z_y-\mu_{y,i})}{\sigma_{x,i}\sigma_{y,i}} \right] \right). \tag{3}$$

By defining a 2×1 measurement vector $\mathbf{z}$ as shown in (4), (3) can be written in matrix notation as shown in (5), where $\boldsymbol{\mu}_{\mathbf{x},i}$ is the 2×1 mean vector and $\Sigma_{\mathbf{x},i}$ is the 2×2 covariance matrix shown in (6). Note that the symbol $|\cdot|$ represents the matrix determinant

$$\mathbf{z} = \begin{bmatrix} z_x \\ z_y \end{bmatrix} \tag{4}$$

$$p_i(\mathbf{z}|\mathbf{x}) = \frac{1}{2\pi\sqrt{|\Sigma_{\mathbf{x},i}|}} e^{-\frac{1}{2}(\mathbf{z}-\boldsymbol{\mu}_{\mathbf{x},i})^T \Sigma^{-1}_{\mathbf{x},i}(\mathbf{z}-\boldsymbol{\mu}_{\mathbf{x},i})} \tag{5}$$

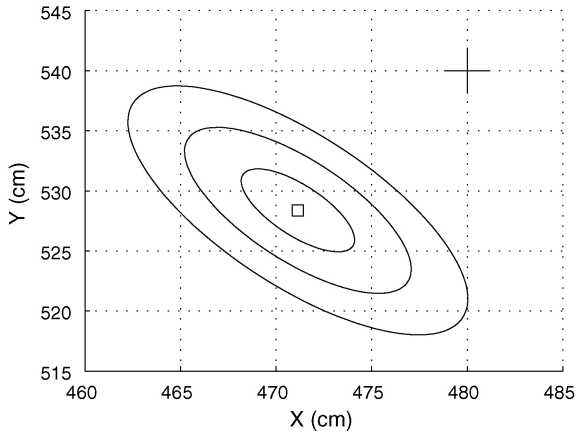

Fig. 6. Model generated from example measurements collected at (480, 540) cm. The ellipses show one, two, and three standard deviations from the mean for each cluster.

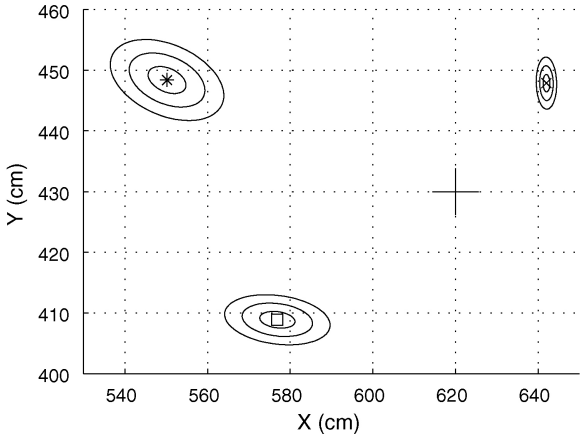

Fig. 7. Model generated from example measurements collected at (620, 430) cm. The ellipses show one, two, and three standard deviations from the mean for each cluster.

$$\Sigma_{\mathbf{x},i} = \begin{bmatrix} \sigma_{x,i}^2 & \rho_{\mathbf{x},i}\sigma_{x,i}\sigma_{y,i} \\ \rho_{\mathbf{x},i}\sigma_{x,i}\sigma_{y,i} & \sigma_{y,i}^2. \end{bmatrix}. \tag{6}$$

Using 3, the PDF of $\boldsymbol{\nu}$ can be defined as shown in (7) where $I_{x,y}$ is the number of modes and $\omega_{x,y,i}$ is the weight value associated with the ith mode. The $\omega_{x,y,i}$ values must sum to one for $p_{\boldsymbol{\nu}}(z_x, z_y|x, y)$ to be a valid PDF

$$p_{\boldsymbol{\nu}}(z_x, z_y|x, y) = \sum_{i=1}^{I_{x,y}} \omega_{x,y,i} \cdot p_i(z_x, z_y|x, y). \tag{7}$$

This can be written in matrix notation as shown in (8), where $\omega_{\mathbf{x},i}$ is the weight and $I_{\mathbf{x}}$ is the number of modes

$$p_{\boldsymbol{\nu}}(\mathbf{z}|\mathbf{x}) = \sum_{i=1}^{I_{\mathbf{x}}} \omega_{\mathbf{x},i} \cdot p_i(\mathbf{z}|\mathbf{x}). \tag{8}$$

E. Generating the Measurement Noise Map

We assume that there exists a PDF, $p_{\boldsymbol{\nu}}(\mathbf{z}|\mathbf{x})$, described by (8), for each possible location within the trackable area of a test facility. To approximate the continuous distribution, we collected measurements at discrete locations as described in Section II-C. We assume local similarity of the measurement noise between discrete locations. The model parameters that are calculated for each location make up the measurement noise map.

Equation (8) requires that four parameters be calculated from the collected measurements: $I_{\mathbf{x}}$, $\boldsymbol{\mu}_{\mathbf{x},i}$, $\Sigma_{\mathbf{x},i}$ and $\omega_{\mathbf{x},i}$. We determine these values using the density-based spatial clustering for applications with noise (DBSCAN) algorithm [30]. This algorithm was selected because it does not require the number of clusters to be specified a priori, as is the case for other common data clustering algorithms, such as K-means. DBSCAN requires two parameters: ϵ, the neighborhood size and k, the minimum number of points necessary to be considered a cluster.

DBSCAN automatically determines $I_{\mathbf{x}}$, the number of clusters present in the data at the location given by $\mathbf{x}$. The cluster mean vector, $\boldsymbol{\mu}_{\mathbf{x},i}$ is calculated for each cluster $i = 1, 2, \ldots, I_{\mathbf{x}}$ found by DBSCAN using (9), where x and y are the location components of the state space variable $\mathbf{x}$, $\mathbf{z}_i^n$ is the nth 2×1 measurement vector assigned to cluster i from the estimates collected at location (x, y) cm. $N_{\mathbf{x},i}$ denotes the number of measurements collected at location (x, y) cm that are assigned to cluster i

$$\boldsymbol{\mu}_{\mathbf{x},i} = \begin{bmatrix} \mu_{x,i} \\ \mu_{y,i} \end{bmatrix} = \frac{1}{N_{\mathbf{x},i}} \left(\sum_{n=1}^{N_{\mathbf{x},i}} \mathbf{z}_i^n \right) . - \begin{bmatrix} x \\ y \end{bmatrix}. \tag{9}$$

$\Sigma_{\mathbf{x},i}$ is the 2×2 unbiased covariance matrix for cluster i at the location given by $\mathbf{x}$ and is calculated as shown in

$$\Sigma_{\mathbf{x},i} = \frac{1}{N_{\mathbf{x},i} - 1} \sum_{n=1}^{N_{\mathbf{x},i}} (\mathbf{z}_i^n - \boldsymbol{\mu}_{\mathbf{x},i})(\mathbf{z}_i^n - \boldsymbol{\mu}_{\mathbf{x},i})^T. \tag{10}$$

The final parameter, $\omega_{\mathbf{x},i}$, is a weight value associated with cluster i at the location given by $\mathbf{x}$. It is calculated by dividing the number of measurements assigned to the cluster by the total number taken at that location, N, as shown in

$$\omega_{\mathbf{x},i} = \frac{N_{\mathbf{x},i}}{N}. \tag{11}$$

Contour plots of the measurement noise model generated for the example set of position estimates shown previously in Figs. 4 and 5 are shown in Figs. 6 and 7, respectively. The contour lines are at one, two, and three standard deviations from the mean.

F. Dynamic Model

For tracking purposes, we use a 2-D constant velocity dynamic model. Equation (12) shows the state space variable $\mathbf{x}_t$ for this type of model. It has four components: the 2-D position at time t, x_t, and y_t, and the 2-D velocity at time t, $\dot{x}_t$, and $\dot{y}_t$

$$\mathbf{x}_t = \begin{bmatrix} x_t \\ \dot{x}_t \\ y_t \\ \dot{y}_t. \end{bmatrix}. \tag{12}$$

Equation (13) gives the function $\mathbf{f}$ that governs state transitions for this model, where δ_t is the sensing interval and σ_d is

the standard deviation of the zero mean, normally distributed dynamic noise. Throughout this paper, the sensing interval is assumed to be 1. From $\mathbf{f}$, the state space equations for this model can be written as shown in (14)

$$\mathbf{f} = \begin{bmatrix} x_t = x_{t-1} + \delta t \cdot \dot{x}_{t-1} \\ \dot{x}_t = \dot{x}_{t-1} + \mathcal{N}(0, \sigma_d) \\ y_t = y_{t-1} + \delta t \cdot \dot{y}_{t-1} \\ \dot{y}_t = \dot{y}_{t-1} + \mathcal{N}(0, \sigma_d) \end{bmatrix} \tag{13}$$

$$\mathbf{x}_t = \mathbf{f}(\mathbf{x}_{t-1}, \sigma_d). \tag{14}$$

G. Basic Particle Filter

The particle filter is a technique for implementing recursive Bayesian estimation through Monte Carlo approximation [31], [32]. It has become a popular alternative to the Kalman and extended Kalman filters for applications with non-Gaussian noise [33]. We use a particle filter framework that incorporates a map of pre-observed measurement noise. This allows the filter to adapt to local variations.

The basic particle filter (BPF) approximates complex distributions using a set of particles. A set of particles is a collection of M state space variables with a weight assigned to each [31]. A distribution is approximated by a set of particles χ, shown in 15, where M is the number of particles, $\mathbf{x}_t^m$ is the state of particle m, and w_t^m is the weight assigned to particle m, both at time t

$$\chi = \{\mathbf{x}_t^m, w_t^m\}_{m=1}^M. \tag{15}$$

The particle states are updated according to the state transition equation $\mathbf{f}$ as shown in (13). The prior importance function is chosen to simplify the sequential importance sampling weight update equation to that shown in (16) where w_{t-1}^m is the weight of particle m at time $t-1$ and $p(\mathbf{z}_t|\mathbf{x}_t^m)$ is the probability of the position estimate, $\mathbf{z}_t$, given the state of particle m, all at time t

$$w_t^m = w_{t-1}^m \cdot p(\mathbf{z}_t|\mathbf{x}_t^m). \tag{16}$$

A 2-D normal distribution with mean at $\boldsymbol{\mu}_{\mathbf{x}_t^m}$ and covariance matrix, Σ_n, is used as the measurement noise model and is calculated as shown in (17). In the BPF, the mean vector, $\boldsymbol{\mu}_{\mathbf{x}_t^m}$, is simply the current particle state. The covariance matrix, Σ_n, is 2×2 and is calculated based on the overall variance of the data collected in the x and y directions. It is assumed that the correlation is 0

$$p(\mathbf{z}_t|\mathbf{x}_t^m) = \frac{1}{2\pi\sqrt{|\Sigma_n|}} e^{-\frac{1}{2}(\mathbf{z}_t - \boldsymbol{\mu}_{\mathbf{x}_t^m})^T \Sigma_n^{-1} (\mathbf{z}_t - \boldsymbol{\mu}_{\mathbf{x}_t^m})}. \tag{17}$$

Next, the particle weights are normalized and the expected value is computed using (18) and (19), respectively. Finally, the coefficient of variation (CV) and effective sample size (ESS) are computed [34] and resampling is performed if necessary. The sampling method that we have chosen is referred to as select with replacement by Rekleitis in [35]

$$w_t^m = \frac{w_t^m}{\sum_{\hat{m}=1}^M w_t^{\hat{m}}} \tag{18}$$

$$E(\mathbf{x}_t) = \sum_{m=1}^M w_t^m \cdot \mathbf{x}_t^m. \tag{19}$$

The CV and ESS are calculated according to (20) and (21). Throughout this paper, resampling is performed when the ESS is determined to be less than $0.5 \times M$, i.e., half of the particle weights have gone to zero

$$ESS = \frac{M}{1 + CV} \tag{20}$$

$$CV = \frac{1}{M} \sum_{m=1}^M \left(M \cdot w_t^m - 1\right)^2. \tag{21}$$

H. Measurement Noise Map Augmented Particle Filter

This paper proposes the use of a measurement noise map, described in Section II-E, within the weight update phase of the BPF. We will refer to this as the measurement noise map augmented particle filter (MNMAPF). The use of a weighted sums of Gaussians to approximate multimodal noise distributions in a particle filter was previously considered in [29], where examples were shown for both dynamic and measurement noise. Our filter is similar to this approach in that it uses weighted sums of Gaussians to approximate multimodal measurement noise distributions. However, our approach uses a facility-wide map to account for location-dependent differences in measurement noise. It is important to note that our map-based method can be used with measurement noise models other than sums of Gaussians. Furthermore, our method could be applied to problems other than UWB position tracking. The key is to capture location-dependent differences in measurement noise in the map prior to filtering and then apply it as shown here.

The measurement noise model used in the weight update step of the MNMAPF is selected from the measurement noise map based on the location components of the mth particle's state. More simply stated, the model parameters for the map position nearest to the particle location are used in the weight update step. Equations (22) and (23) show analytically how $p(\mathbf{z}_t|\mathbf{x}_t^m)$ is generated using our map-based measurement noise model where $p_i(\mathbf{z}_t|\mathbf{x}_t^m)$ is the unimodal Gaussian PDF for each cluster at the map location nearest $\mathbf{x}_t^m$

$$p(\mathbf{z}_t|\mathbf{x}_t^m) = p_{\boldsymbol{\nu}}(\mathbf{z}_t|\mathbf{x}_t^m) = \sum_{i=1}^{I_{\mathbf{x}}} \omega_{\mathbf{x}_t^m,i} \cdot p_i(\mathbf{z}_t|\mathbf{x}_t^m). \tag{22}$$

$$p_i(\mathbf{z}_t|\mathbf{x}_t^m) = \frac{1}{2\pi\sqrt{|\Sigma_{\mathbf{x}_t^m,i}|}} e^{-\frac{1}{2}(\mathbf{z}_t - \boldsymbol{\mu}_{\mathbf{x}_t^m,i})^T \Sigma_{\mathbf{x}_t^m,i}^{-1} (\mathbf{z}_t - \boldsymbol{\mu}_{\mathbf{x}_t^m,i})}. \tag{23}$$

I. Error Metric

The metric that will be used to compare filter performance throughout this paper is referred to as the average error e and is calculated using the Euclidean distance between a ground truth location and the corresponding filter output. The calculation is performed as shown in (24), where x_n and y_n are the nth

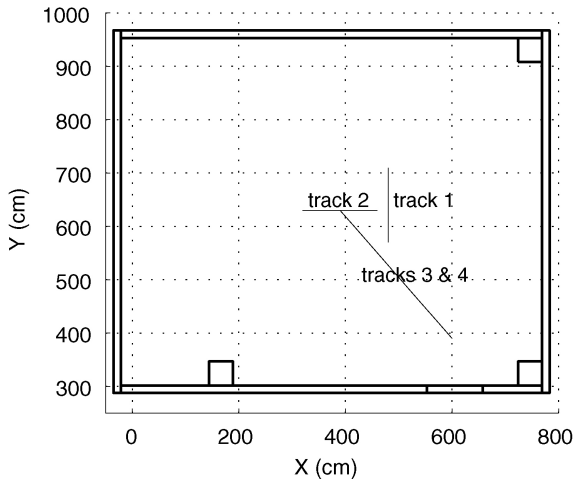

Fig. 8. Plot of the ranges covered by tracks 1–4.

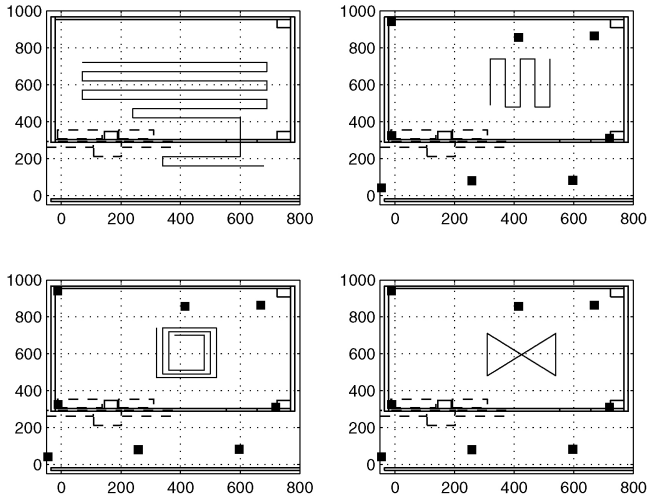

Fig. 9. Plot of the ranges covered by tracks 5 (top left), 6 (top right), 7 (bottom left), and 8 (bottom right).

filter output, and $\hat{x}_n$ and $\hat{y}_n$ are the corresponding ground truth location

$$e = \frac{1}{N}\sum_{n=1}^{N}\sqrt{(x_n - \hat{x}_n)^2 + (y_n - \hat{y}_n)^2}. \tag{24}$$

J. Dynamic Track Collection

Eight tracks were defined within the trackable area of the Riggs facility. Figs. 8 and 9 show plots of each track within the Riggs facility. There are five recordings of tracks 1, 2, and 4 and four of track 3. Tracks 3 and 4 cover the same ground truth coordinates; track 3 runs northwest and track 4 runs southeast.

Tracks 1 and 2 were collected by dragging the UWB tag across the top of a saw horse. It was placed at a known ground truth location within the trackable area. Tracks 3 and 4 were collected by placing the UWB tag on a cart. The cart was then moved along a known ground truth path. Tracks 5–8 were generated by randomly pulling position estimates from the dense collection data. This was done to increase the overall

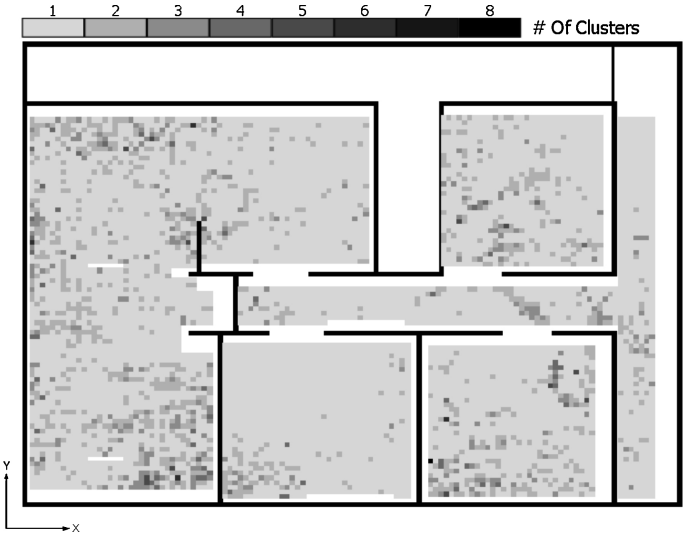

Fig. 10. Contour plot of the number of clusters determined by the DBSCAN algorithm at each measurement location within the Shoothouse facility; ϵ = 30 cm and k = 10.

number of recordings considered, but due to changes to the Ubisense system configuration in the intervening months to support an additional research project on installation optimization, no further recordings could be made. These tracks are much longer and more complicated than tracks 1–4. They all help to demonstrate the proposed method.

III. Results

A. Measurement Noise

Figs. 10 and 11 show maps of the number of clusters determined by the DBSCAN algorithm at all measurement locations within the test facilities. It can be seen that the measurement noise sometimes contains only one cluster but that multiple clusters occur near walls and the boundaries of the trackable area. More specifically, 68% of the locations surveyed have a single cluster. This type of measurement noise behavior is taken into account by the use of a multimodal Gaussian model.

Figs. 12 and 13 show the average error vector for every fourth collection location in each facility. It can be seen that measurements taken at different areas are biased away from the ground truth location in different directions and with different magnitudes. The proposed map-based measurement noise model accounts for this location-dependent bias.

B. Stability Over Time

The validity of the measurement noise model developed in this paper depends on the assumption that the measurement noise remains relatively constant over time. If the noise changes significantly from hour to hour or day to day, the model calculated from measurements collected at a specific time will no longer be valid at a later date. To test for stability over time, we took measurements in a subset of the trackable area of the Riggs facility over two months to compare the measurement noise models over time. Measurements were

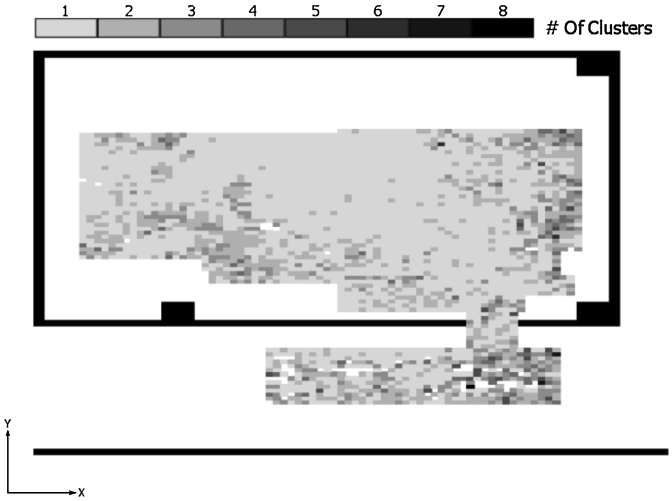

Fig. 11. Contour plot of the number of clusters determined by the DBSCAN algorithm at each measurement location within the Riggs facility; $\epsilon = 30$ cm and $k = 10$.

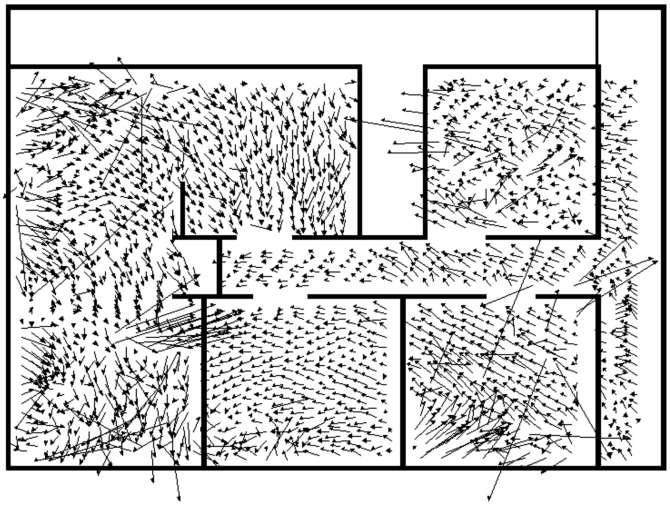

Fig. 12. Plot of error vectors in the Shoothouse facility.

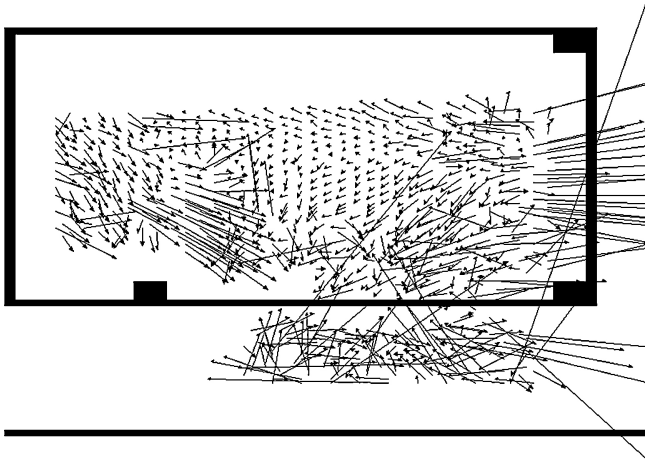

Fig. 13. Plot of error vectors in the Riggs facility.

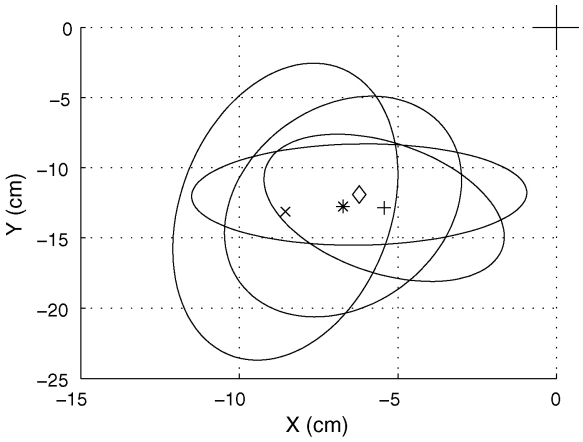

Fig. 14. Zoomed-in plot of model data collected on three consecutive days and then again two months later. The cluster means are indicated by the +, *, x and diamond symbols.

collected in 10-cm intervals as described in Section II-C in the range of (310–470, 540–630) cm on three consecutive days and then again two months later. Fig. 14 is a plot of the model generated for measurements collected at (470, 590) cm on these four days. It can be seen from this figure that all cluster means (+, *, x and diamond symbols) are south and west of the ground truth location, denoted by the large cross symbol in the upper right. The ellipses shown are each three standard deviations from the respective mean according to the sample covariance matrices and can be seen to significantly overlap one another. Fig. 14 is representative of the type of change in model that we observed across the area surveyed. The average change in cluster mean over time was 3.7 cm with a standard deviation of 3.1 cm. This is small compared to the average error, which is approximately 20 cm.

C. Local Similarity

Local similarity refers to the differences in measurement noise from one position to another within a small area. We use the model for the collection location closest to the state as the model for that state because we do not have model data for all possible states. We assume that the measurement noise does not change significantly across a small area, i.e., within 10 cm. To test this assumption, we took measurements at 1-cm intervals in a subset of the Riggs facility and compared them to determine the validity of the local similarity assumption. Fig. 15 is a plot of four sets of model data. The model indicated by the small cross symbol is the one measured at the given location. The model indicated by the asterisk is the model from the nearest collection location on the measurement noise map. It can be seen that the means from all four locations are close to each other and that there is significant overlap of the ellipses. While this is a limited test, it does provide some confidence in the assumption of local similarity.

D. Filtering Results

Table I shows the average error for ten iterations of the BPF and MNMAPF for each of the eight tracks. The tracks show a range of velocities and as has been shown previously, cover much of the facility. The MNMAPF has an average error approximately 30% less than the average raw and BPF

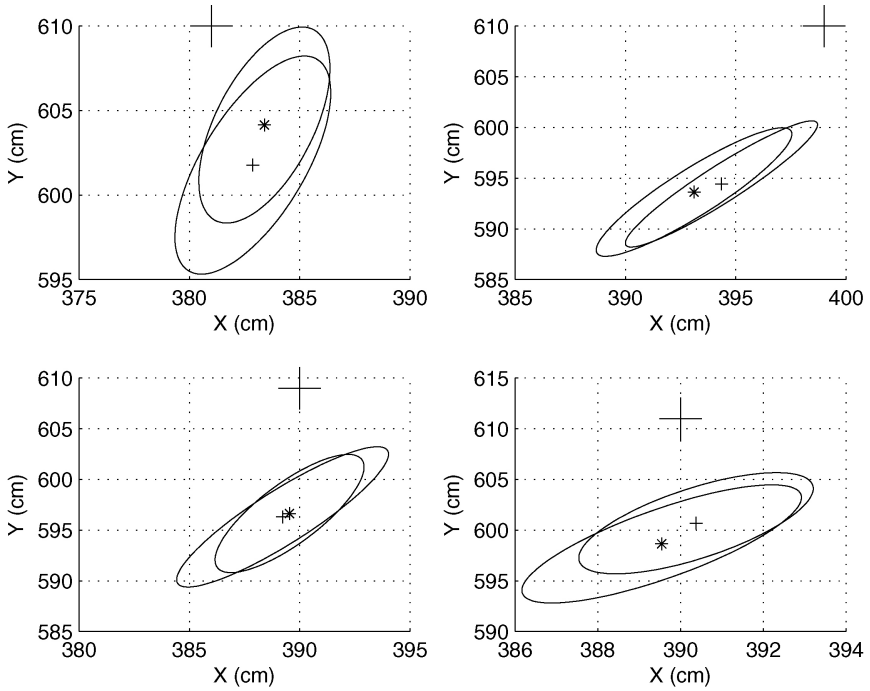

Fig. 15. Zoomed-in plot of the measured model (small cross) and adjusted model (asterisk) at (381, 610), (399, 610), (390, 609), (390, 611) cm in the top left, top right, bottom left and bottom right, respectively.

TABLE I
COMPARISON OF LENGTH, VELOCITY, AVERAGE RAW ERROR, AVERAGE BPF ERROR, AND AVERAGE MNMAPF ERROR FOR ALL EIGHT RECORDINGS

Trial	Length (cm)	Velocity (cm/s)	# Points	Raw Error (cm)	BPF Error (cm)	MNMAPF Error (cm)
1	140	20	68	10	9	6
2	140	16	73	14	11	7
3	210	76	43	35	35	29
4	210	70	43	28	29	18
5	3800	90	380	35	35	19
6	1520	90	152	18	19	10
7	2320	90	232	20	20	17
8	1090	90	188	24	24	19

measurement errors for all tracks. Because the particle filter is based on Monte Carlo simulation, single applications of the BPF and MNMAPF do not give a good indication of the type of results that can be achieved. Therefore, the error is averaged over ten iterations.

IV. CONCLUSION

This paper presented methods for building a map of UWB measurement noise and using it in a particle filter framework to improve indoor position tracking accuracy. Through two collection campaigns, UWB measurement noise was shown to be location dependent and multimodal. To account for this multimodality, noise at a specific location was modeled using a sum of Gaussians. Evidence was shown that the measurement noise was stable over time and locally similar. Finally, a 30% reduction in tracking error was shown through the use of the measurement noise map in the context of a particle filter.

A limitation of our method is the requirement that the measurement noise map be re-calculated after a significant change to the positioning system installation or environment occurs. Because of this, it is expected that this type of map would be generated for a system once and used for a long period of time. Furthermore, we acknowledged that a significant time commitment was required to generate the measurement noise map. The development of more automated methods to generate the measurement noise map could significantly reduce this time commitment and allow for the measurement noise model to be recalculated on a more frequent basis if necessary. It may be that floor plan and sensor geometry information could be used to semi-automate this process similar to the techniques shown in [36] and [37]. This is a subject of future work.

REFERENCES

[1] N. Patwari, J. Ash, S. Kyperountas, A. O. Hero, R. Moses, and N. Correal, "Locating the nodes," *IEEE Signal Process. Mag.*, vol. 22, no. 4, pp. 54–69, Jul. 2005.

[2] A. Sayed, A. Tarighat, and N. Khajehnouri, "Network-based wireless location," *IEEE Signal Process. Mag.*, vol. 22, no. 4, pp. 24–40, Jul. 2005.

[3] D. Dardari, A. Conti, U. Ferner, A. Giorgetti, and M. Z. Win, "Ranging with ultrawide bandwidth signals in multipath environments," *Proc. IEEE*, vol. 97, no. 2, pp. 404–426, Feb. 2009.

[4] W. Chung and D. Ha, "An accurate ultrawideband (UWB) ranging for precision asset location," in *Proc. Int. Conf. Ultra Wideband Syst. Technol.*, 2003, pp. 389–393.

[5] Y. Qi, H. Kobayashi, and H. Suda, "Analysis of wireless geolocation in a non-line-of-sight environment," *IEEE Trans. Wireless Commun.*, vol. 5, no. 3, pp. 672–681, Mar. 2006.

[6] B. Waldmann, A. Goetz, and R. Weigel, "An ultrawideband positioning system enhanced by a short multipath mitigation technique," in *Proc. IEEE MTT-S Int. Microwave Workshop Wireless Sens., Local Position., RFID*, 2009, pp. 1–4.

[7] M. J. Kuhn, J. Turnmire, M. R. Mahfouz, and A. E. Fathy, "Adaptive leading-edge detection in UWB indoor localization," in *Proc. IEEE Radio Wireless Symp.*, Jan. 2010, pp. 268–271.

[8] R. Ye, S. Redfield, and H. Liu, "High-precision indoor UWB localization: Technical challenges and method," in *Proc. IEEE Int. Conf. Ultra Wideband*, Sep. 2010, pp. 1–4.
[9] M. Mahfouz, C. Zhang, B. Merkl, M. Kuhn, and A. Fathy, "Investigation of high-accuracy indoor 3-D positioning using UWB technology," *IEEE Trans. Microwave Theor. Techniques*, vol. 56, no. 6, pp. 1316–1330, Jun. 2008.
[10] Y. Zhou, C. L. Law, Y. L. Guan, and F. Chin, "Indoor elliptical localization based on asynchronous UWB range measurement," *IEEE Trans. Instrum. Meas.*, vol. 60, no. 1, pp. 248–257, Jan. 2011.
[11] C. Morelli, M. Nicoli, V. Rampa, and U. Spagnolini, "Hidden Markov models for radio location in mixed LOS/NLOS conditions," *IEEE Trans. Signal Process.*, vol. 55, no. 4, pp. 1525–1542, Apr. 2007.
[12] B. Denis, L. Ouvry, B. Ulguen, and F. Tchoffo-Talom, "Advanced Bayesian filtering techniques for UWB tracking systems in indoor environments," in *Proc. IEEE Int. Conf. Ultrawideband*, 2005, pp. 638–643.
[13] J. Youssef, B. Denis, C. Godin, and S. Lesecq, "Enhanced linearized location estimators with optimization-based combinations of radiolocation measurements," in *Proc. IEEE 20th Int. Symp. Personal, Indoor Mobile Radio Commun.*, Sep. 2009, pp. 2055–2059.
[14] D. Jourdan, D. Dardari, and M. Win, "Position error bound for UWB localization in dense cluttered environments," *IEEE Trans. Aerosp. Electron. Syst.*, vol. 44, no. 2, pp. 613–628, Apr. 2008.
[15] S. Martínez and F. Bullo, "Optimal sensor placement and motion coordination for target tracking," *Automatica*, vol. 42, no. 4, pp. 661–668, 2006.
[16] B. Gozick, K. P. Subbu, R. Dantu, and T. Maeshiro, "Magnetic maps for indoor navigation," *IEEE Trans. Instrum. Meas.*, vol. 60, no. 12, pp. 3883–3891, Dec. 2011.
[17] C. Steiner and A. Wittneben, "Low complexity location fingerprinting with generalized UWB energy detection receivers," *IEEE Trans. Signal Process.*, vol. 58, no. 3, pp. 1756–1767, Mar. 2010.
[18] S.-H. Fang and T.-N. Lin, "Indoor location system based on discriminant-adaptive neural network in IEEE 802.11 environments," *IEEE Trans. Neural Netw.*, vol. 19, no. 11, pp. 1973–1978, Nov. 2008.
[19] F. Gustafsson, F. Gunnarsson, N. Bergman, U. Forssell, J. Jansson, R. Karlsson, and P.-J. Nordlund, "Particle filters for positioning, navigation, and tracking," *IEEE Trans. Signal Process.*, vol. 50, no. 2, pp. 425–437, Feb. 2002.
[20] R. Karlsson and F. Gustafsson, "Bayesian surface and underwater navigation," *IEEE Trans. Signal Process.*, vol. 54, no. 11, pp. 4204–4211, Nov. 2006.
[21] A. Paul and E. Wan, "RSSI-based indoor localization and tracking using sigma-point Kalman smoothers," *IEEE J. Select. Topics Signal Process.*, vol. 3, no. 5, pp. 860–873, Oct. 2009.
[22] P. Davidson, J. Collins, and J. Takala, "Application of particle filters for indoor positioning using floor plans," in *Proc. IEEE Int. Conf. Exhibition Ubiquitous Positioning, Indoor Navigation, Location Based Service*, Oct. 2010, pp. 1–4.
[23] A. Hoover and E. Muth, "Instrumenting for measuring," in *The PSI Handbook of Virtual Environments for Training and Education*, vol. 3. Techlink, Singapore: Praeger Security International Publishing, 2008, pp. 184–195.
[24] A. Elkins, E. Muth, A. Hoover, A. Walker, T. Carpenter, and F. Switzer, "Physiological compliance and team performance," *Appl. Ergonom.*, vol. 40, no. 6, pp. 997–1003, Nov. 2009.
[25] Ubisense, Inc. (2011, May). *Ubisense Precise Location* [Online]. Available: http://www.ubisense.net/en/resources/factsheets/ubisense-precise-locati%on.html
[26] Ubisense, Inc., (2008). LocationEngineConfig User Manual [Online]. Available: http://www.parl.clemson.edu/ wsuski/UbisenseLocationEngineConfig.pdf
[27] M. J. Kuhn, M. R. Mahfouz, J. Turnmire, Y. Wang, and A. E. Fathy, "A multi-tag access scheme for indoor UWB localization systems used in medical environments," in *Proc. IEEE Topical Conf. Biomed. Wireless Technol., Netw., Sens. Syst.*, Jan. 2011, pp. 75–78.
[28] H. Sorenson and D. Alspach, "Recursive Bayesian estimation using Gaussian sums," *Automatica*, vol. 7, pp. 465–479, 1971.
[29] J. Kotecha and P. Djurić, "Gaussian sum particle filtering," *IEEE Trans. Signal Process.*, vol. 51, no. 10, pp. 2602–2612, Oct. 2003.
[30] M. Ester, H. Kriegel, J. Sander, and X. Xu, "A density-based algorithm for discovering clusters in large spatial databases with noise," in *Proc. 2nd Int. Conf. Knowl. Discovery Data Mining*, 1996, pp. 226–231.
[31] S. Arulampalam, S. Maskell, N. Gordon, and T. Clapp, "A tutorial on particle filters for online nonlinear/non-Gaussian Bayesian tracking," *IEEE Trans. Signal Process.*, vol. 50, no. 2, pp. 174–188, Feb. 2002.
[32] A. Doucet, S. Godsill, and C. Andrieu, "On sequential Monte Carlo sampling methods for Bayesian filtering," *Stat. Comput.*, vol. 10, no. 3, pp. 197–208, 2000.
[33] P. Djurić, J. Kotecha, J. Zhang, Y. Huang, T. Ghirmai, M. Bugallo, and J. Miguez, "Particle filtering," *IEEE Signal Process. Mag.*, vol. 20, no. 5, pp. 19–38, Sep. 2003.
[34] J. S. Liu, R. Chen, and T. Logvinenko, "A theoretical framework for sequential importance sampling and resampling," in *Sequential Monte Carlo in Practice*, A. Doucet, N. de Freitas, and N. Gordon, Eds. Berlin, Germany: Springer-Verlag, Jan. 2001.
[35] I. M. Rekleitis, "A particle filter tutorial for mobile robot localization," Centre Intelligent Machines, McGill Univ., Tech. Rep. TR-CIM-04-02, 2002.
[36] M. Nicoli, C. Morelli, and V. Rampa, "A jump Markov particle filter for localization of moving terminals in multipath indoor scenarios," *IEEE Trans. Signal Process.*, vol. 56, no. 8, pp. 3801–3809, Aug. 2008.
[37] T. Roos, P. Myllymaki, and H. Tirri, "A statistical modeling approach to location estimation," *IEEE Trans. Mobile Comput.*, vol. 1, no. 1, pp. 59–69, Jan.–Mar. 2002.

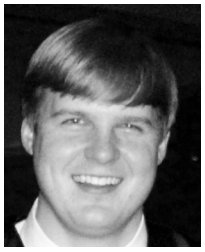

William Suski (S'12) received the B.S. degree in computer engineering from Clemson University, Clemson, SC, USA, in 2005, and the M.S. degree in electrical engineering from the Air Force Institute of Technology, Ohio, USA, in 2008. In 2009, he returned to Clemson University to pursue the Ph.D. degree in electrical engineering, which he completed in 2012.

His current research interests include radio frequency fingerprinting, tracking systems, pattern recognition, and software-defined radio.

Salil Banerjee (S'05) received the B.S. degree in electronics engineering from Mumbai University, Mumbai, India, in 2004. He is currently pursuing the Ph.D. degree in electrical engineering at Clemson University, Clemson, SC, USA. His doctoral research focuses on the development of noise models and improving tracking in an ultrawideband based local positioning system.

His current research interests include tracking systems, image processing, behavioral biometrics, and pattern recognition.

Adam Hoover (M'96–SM'06) received the B.S. and M.S. degrees in computer engineering and the Ph.D. degree in computer science and engineering from the University of South Florida, Tampa, FL, USA, in 1992, 1993, and 1996, respectively.

From 1996 to 1998, he was a Post-Doctoral Researcher with the Electrical and Computer Engineering Department, University of California, San Diego, CA, USA. In 1999, he joined the Electrical and Computer Engineering Department, Clemson University, Clemson, SC, USA, where he is currently an Associate Professor. His current research interests include tracking systems and embedded systems.